Dynamic acousto-elastic test using continuous probe wave and transient vibration to investigate material nonlinearity

J.N. Eiras[a*], Q.A. Vu[b], M. Lott[b], J. Payá[a], V. Garnier[b], C. Payan[b]

[a] Instituto de Ciencia y Tecnología del Hormigón (ICITECH), Universitat Politècnica de València, Camino de Vera s/n, 46022 València, Spain

[b] Aix-Marseille Université, LMA UPR 7051, IUT, 413 Av. Gaston Berger, 13100 Aix-en-Provence, France

Abstract

This study demonstrates the feasibility of the dynamic acousto-elastic effect of a continuous high frequency wave for investigating the material nonlinearity upon transient vibration. The approach is demonstrated on a concrete sample measuring 15x15x60 cm^3. Two ultrasonic transducers (emitter and receiver) are placed at its middle span. A continuous high frequency wave of 500 kHz propagates through the material and is modulated with a hammer blow. The position of the hammer blow on the sample is configured to promote the first bending mode of vibration. The use of a continuous wave allows discrete time extraction of the nonlinear behavior by a short-time Fourier transform approach, through the simultaneous comparison of a reference non-modulated signal and an impact-modulated signal. The hammer blow results in phase shifts and variations of signal amplitude between reference and perturbed signals, which are driven by the resonant frequency of the sample. Finally, a comprehensive analysis of the relaxation mechanisms (modulus and attenuation recovery) is conducted to untangle the coupled fast and slow hysteretic effects.

[*]Author to whom correspondence should be addressed; electronic mail: jeseifer@posgrado.upv.es

1. Introduction

Investigation of the nonlinear dynamic properties of materials and structures is attracting keen interest among several scientific communities such as geosciences[1], medicine[2], and materials science[3], thanks to their improved detection of microstructural features within materials[4]. The link between the concerned materials among the different research areas is the presence of defects in a wide range of scales (from nano- to macro-scale), which enhances the nonlinear acoustic phenomena[5–7]. The internal friction between rough interfaces in their imperfect microstructures causes a hysteretic behavior in terms of their quasi-static stress-strain relationships. The resulting nonlinear modulus (M) including mechanical hysteresis can be written as[5]

$$M = M_o\left[1 + \beta\varepsilon + \delta\varepsilon^2 + \ldots + U\left(\Delta\varepsilon, \dot{\varepsilon}\right)\right], \qquad (1)$$

where the linear elastic modulus (M_o) is extended to include classical elastic higher order terms of strain, β and δ, and a function that takes account of mechanical hysteresis; usually written as[8]

$$U\left(\Delta\varepsilon, \dot{\varepsilon}\right) = \alpha \cdot \left(\Delta\varepsilon + \varepsilon \cdot sign(\dot{\varepsilon})\right), \qquad (2)$$

where α is a parameter that controls the magnitude of the hysteretic behavior, $\Delta\varepsilon$ is the strain amplitude, ε is strain, and $\dot{\varepsilon}$ is strain rate. Under moderate dynamic strain amplitudes, ~10^{-7} and above[9], the hysteretic behavior is manifested as an apparent softening of the material, so-called non-classical behavior. The velocity of propagation and attenuation of the material depend on the strain amplitude (fast dynamic effect), which in turn is accompanied by a long period of relaxation after dynamic excitation (slow dynamic effect). The two mechanisms are thought to coexist during dynamic excitation (material conditioning)[10], and dominate the nonlinear behavior of highly heterogeneous media such as those in concrete-like materials[11]. The equation of state as presented in Eq. 1 falls short of describing the slow dynamic effect, and only the fast dynamic effect can be considered therein[11]. The fast dynamic effect has been broadly investigated through nonlinear resonant techniques. They consist in the investigation of the downward resonant frequency shift observed in consecutive acquisitions by increasing the excitation amplitude[8]. The normalized downward resonant frequency shift is in most materials proportional to the strain amplitude[10] and is related to the parameter α because of the fast dynamic effect as[8]

$$\frac{\Delta f}{f_o} = \alpha \cdot \Delta \varepsilon , \quad (3)$$

where f_o is the resonant frequency obtained in the linear strain regime. Therefore, the investigation of the material nonlinearity through nonlinear resonant spectroscopy-based techniques relies on the fast dynamic effect (Eq.3), and the unavoidable effect of slow dynamics contributes to the error in the estimation of the parameter α [10,11]. Such an effect is normally minimized by increasing the time lapse between successive resonant frequency acquisitions.

Recent research on the application of nonlinear acoustics for the characterization of biological tissues allowed investigation of the whole range of nonlinear phenomena with the technique termed dynamic acousto-elastic test (DAET)[12]. The DAET consists in monitoring the variations of the speed of sound through the material, normally through variations in the time of flight of ultrasonic pulses (probe wave), while a low frequency burst that matches a fundamental resonant mode perturbs the media (pump wave). Assuming that Poisson's ratio, and density variations are negligible during pump wave excitation, the resulted variations of modulus are related to the speed of sound (c) as

$$\frac{M - M_o}{M_o} \approx \frac{c^2 - c_o^2}{c_o^2}. \tag{4}$$

Considering that the variations of the speed of sound (Δc) with respect to the speed of sound in the linear elastic regime (c_0) are so small that $c \approx c_0$ —and hence, $c^2 - c_0^2 \approx 2 \cdot (c - c_0)$—, the corresponding relative variations of time of flight ($\Delta t/t_o$) are approximately related to the material nonlinearity as[12-14]

$$\frac{M - M_o}{M_o} \approx -2 \cdot \frac{\Delta t}{t_o} \approx C_E(\Delta\varepsilon) + \beta\varepsilon + \delta\varepsilon^2 + \ldots + U(\Delta\varepsilon, \dot{\varepsilon}); \tag{5}$$

where, additional to the quadratic and cubic nonlinear classical parameters (β and δ) and strain rate-dependent hysteresis $U(\Delta\varepsilon, \dot{\varepsilon})$, the function $C_E(\Delta\varepsilon)$ takes into account the material conditioning effect: the apparent mix of slow and fast dynamics[10] which offsets the relation between strain and the relative variation of modulus. In addition, the variations of material attenuation produced during low frequency burst excitation, are also derived from the amplitude of the ultrasonic pulses[12-14].

Two conditions must be accomplished in DAET experiments. First, the time of flight (t_0) of the ultrasonic probe wave must be less than 1/10 times the value of the low frequency excitation[13]. In this way, the instantaneous variations of time of flight can be precisely related to the strain amplitude of the pump wave excitation. Second, the repetition rate of the ultrasonic pulse generator has to be set so that the ultrasonic wave is completely attenuated between pulses. Therefore, the succeeding ultrasonic pulses are not affected by the coda wave of the preceding ones[12-14]. In consequence of the last, the variations of time of flight and amplitude are obtained for few values of strain in several cycles of the low frequency burst (constant strain amplitude excitation). Therefore, the test has to be repeated after changing the phase of the ultrasonic pulse generator to obtain more experimental data, and describe properly the variations of time of flight and amplitude over the whole strain range excitation[12-14]. These conditions make unpractical to leverage the potential of DAET in on-site assessment of structures or in structural health monitoring applications wherein the use of ambient vibrations and transient events (variable strain amplitude excitation) are required to monitor passively the dynamic properties of structures[15-17].

In this study, a DAET is conducted by modulating a continuous monochromatic high frequency probe that propagates through the material. The approach is demonstrated on a prismatic concrete sample. The modulation of the continuous wave signal is achieved by a hammer blow configured to promote its first bending mode of vibration. The signal analysis is conducted with a short-time Fourier transform based approach. It is based on extracting the phase and amplitude variations by the simultaneous comparison between a reference (non-modulated) and an impact-modulated signal. Thus, the changes in velocity in the medium produced upon transient vibration rely on the phase changes of the continuous probe. Unlike previous DAET configurations[13,14,18-20], the approach presented herein has two main advantages. It overcomes the inconvenience of changing the phase of the high frequency probe (in case of ultrasonic pulses) in consecutive experiments for discretizing the variations of wave velocity over the whole range of strain excitation, and it allows investigation of the discrete time variation of material nonlinearity over only one cycle of low frequency excitation. Therefore, the variations of modulus can be investigated during the ring down of the mechanical energy introduced by a hammer blow. Otherwise, when a hammer blow is used as low frequency source and ultrasonic pulses as probe wave[21,22], the only measurable parameter is the maximum offset of the normalized time shift ($\Delta t/t_o$), since the strain amplitude is variable over time. Conversely, the parameters extracted herein show similarity with the nonlinear acoustic behavior derived from Eq.5, and previously observed in compressional mode DAET experiments[13,14,18-20]. These are: 1) an offset of the material modulus upon low frequency excitation, 2) a phase delay between the onset of the strain amplitude and the relative variations of modulus, and 3) an incomplete recovery of the dynamic properties of the material when the strain energy of the low frequency signal is completely damped.

2. Materials and methods

2.1. Materials

The tests were conducted on a concrete sample measuring 15x15x60 cm^3. The composition of concrete is listed in Table 1. At the moment of test, the concrete sample was fully matured. For reference, the compressional and shear wave velocities were determined using direct transmission of an ultrasonic pulse, along the straight-line path respect to the sample width. For compressional wave velocity measurement, two ultrasonic transducers GE-Measurement & Control (model G 0,25 G code 67422, central frequency of 250 kHz) were used. For shear wave velocity measurement, two transducers Panametrics-NDT (model V151, central frequency of 250 kHz) were used. The compressional and shear wave velocities were 4056 m/s and 2483 m/s. The density of the sample was ρ = 2350 kg/m^3; thus *Mo* = 37.8 GPa, and Poisson's ratio ν = 0.20.

Table 1. Mix design of concrete and properties.

Cement CEM I/52.5N (kg/m^3)	370
Water (l/ m^3)	212

Fine aggregates 0/4 (kg/m^3)	774
Coarse aggregates 4/14 (kg/m^3)	1069
Compressive strength at 28 days (MPa)	53

2.2. Experimental configuration

Figure 1 shows a schematic depiction of the experimental configuration. Two ultrasonic transducers (Panametrics-NDT model V101, central frequency of 500 kHz) were placed on the sample at its middle span with a distance (*d*) between them, center to center, of 10 cm. A continuous sinusoidal high frequency probe was modulated by a hammer blow, while an accelerometer (Bruel & Kjaer model 4525B, sensitivity of 1.046 mV/(m.s^{-2})) monitored the out-of-plane acceleration at the center of the sample. The relative position between impact and accelerometer was configured to promote the first bending mode of vibration. The strain amplitude owed to the first bending mode of vibration was derived from the accelerometer response (see section 2.4). An instrumented hammer (Bruel & Kjaer model 8207, sensitivity of 0.230 mV/N) with a polymeric tip was used to perform the measurements. Five different energy impacts were conducted between 1kN to 5kN, which resulted in values of resonant frequency between 1442 Hz and 1440 Hz. The time lapse between different acquisitions was set at one minute.

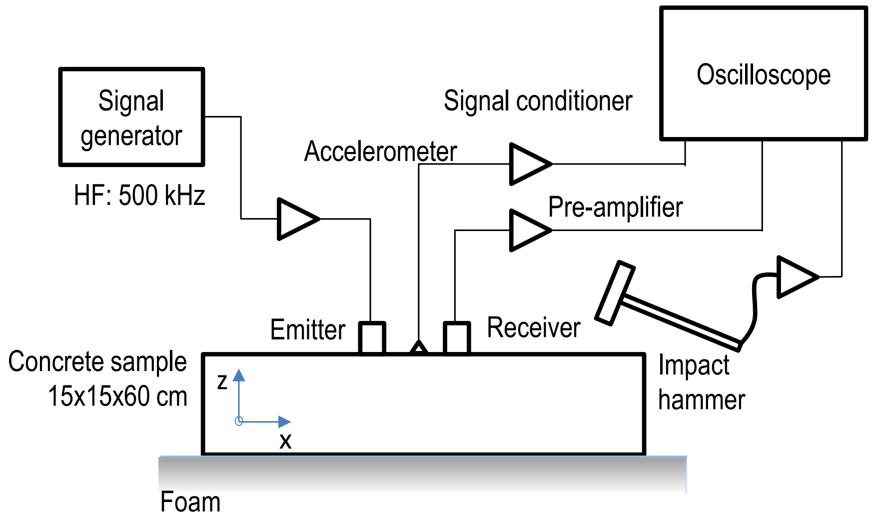

Figure 1. Schematic representation of the experimental setup.

Recently, Fröjd and Ulrikssen[23] investigated the effect of a static load on the amplitude and phase of a continuous wave excitation at 47 kHz. In such study, the authors argued that the continuous wave source produced a steady-state diffuse field which consisted of direct propagation, scattered waves, and reflections from the boundaries of the concrete sample being investigated therein. In this study, the frequency of the continuous ultrasonic probe was set to 500 kHz. At such a frequency, multiple scattering effects occur in concrete and a strong attenuation of the energy in every direction is produced[24,25]. Thus, the resulted field is mainly dominated by direct propagation, but reflection contributions from sample boundaries are dramatically minimized. For reference, the amplitude of the continuous wave excitation in a through-thickness continuous wave measurement was reduced more than 80% that obtained by using the original test configuration (as shown in Figure 1). Therefore, the reflected energy recorded by the receiver in the original position is not a significant contribution to the total received energy. The continuous wave is then perturbed by a hammer blow and as a result, the amplitude and phase of the continuous probe are modulated because of the material nonlinearity.

The distance between the transducers has to be set, so that the instantaneous variations of phase and amplitude can be precisely related to the strain values derived from the acceleration response. Despite, any specific bulk wave can be attributed to the continuous wave excitation, the time of flight obtained for compressional wave was used to meet this requirement. To this end, the distance between the transducers was set to d= 10 cm. Then, indirect propagation (as shown in Figure 1) of five cycles at 500 kHz provided a time of flight of t_o= 26.8 μs (p-wave arrival). This value of t_o ensured that the instantaneous variations of amplitude and phase correspond to less than 1/10 times the period of the low frequency excitation[13]. On other hand, we noticed that the value of t_o was significantly lower than that obtained using direct transmission (see section 2.1). This effect is most likely due to the different material properties in the near-surface regions with respect to the inner core of the concrete samples[26,27].

2.3. Signal processing

The out-of-plane particle displacement because of the continuous monochromatic probe wave before a hammer blow excitation ($y_r(t)$) can be written as

$$y_r(t) = B \cdot \sin(\omega_r \cdot t) \cdot e^{-\gamma_r \cdot d} + \Psi_r(t), \tag{6}$$

where B is the amplitude of the signal, ω_r is the angular frequency of the probe, γ_r is the ultrasonic attenuation, and $\Psi_r(t)$ is a function containing the non-coherent information of the multiple scatters recorded on propagation from the emitter to the receiver. Subscript r stands for “reference”, whereby the ultrasonic probe is assumed to propagate through the medium in the linear elastic regime. Namely, in absence of hammer blow excitation. The high frequency probe $y_r(t)$ is then perturbed by a hammer blow. As a result of the presence of contact-like defects within the imperfect microstructure of concrete, the modulus of the material varies upon compression and tension cycles induced by the pump wave excitation[28]. Then, the phase and amplitude of the probe wave signal are modulated. The resulting impact-modulated signal $y_p(t)$ can be written as

$$y_p(t) = B \cdot \sin(\omega_r \cdot t + \Omega(t)) \cdot e^{-(\gamma_r + \Gamma(t))d} + \Psi_p(t)\,. \qquad (7)$$

The functions $\Omega(t)$ and $\Gamma(t)$ are the phase and amplitude modulation contributions. Both functions must consider the periodic variations of phase and attenuation, as well as the instantaneous offsets produced with the onset of the strain amplitude. Phase and amplitude modulation manifest as sideband peaks with respect to the frequency of the probe wave, when the whole modulated probe signal is transformed to the frequency domain. The relative energy of the sideband components, with respect to the energy of the probe wave, has been used as a measurement of material nonlinearity[28]. However a more detailed description is proposed herein. The variation of material modulus because of the presence of contact-like defects can be quantified through the instantaneous phase difference of the impact-modulated probe (Eq.7) with respect the reference (Eq.6). The resulting instantaneous phase difference between both signals is the function $\Omega(t)$. To this end, a sliding window moves through the time domain signals of the probe waves (Eqs. 6 and 7) and transforms the time segments within the window to the frequency domain. At every windowed time segment (τ), the time shift (Δt) between perturbed and reference signals is obtained from their spectral phases ($\Phi_p(\omega)$ and $\Phi_r(\omega)$) at the probe frequency (ω_r) as

$$\frac{\Delta t|_{\tau}}{t_0} = \frac{\phi_p(\omega)|_{\omega_r} - \phi_r(\omega)|_{\omega_r}}{t_0 \cdot \omega_r}\,. \qquad (8)$$

Given that a continuous probe lacks a clear wave path, and it does not allow extraction of phase velocity, in this study we assume that the time shift variations between reference and modulated signals are related to the variation of the material modulus. Therefore, the relative time shift modulation obtained from Eq. 8 provides insight into the relative variation of the modulus as deduced in Eq. 5. A normalization of the time shift (Δt) by t_0 is still needed, especially when different materials are to be compared[22]. The time of flight obtained for indirect propagation of 5 cycles at 500 kHz was selected as the reference value (t_0= 26.8μs). In addition, at every window position, the variation of the attenuation properties between reference and impact-modulated probe can be considered as[14]

$$\gamma_p - \gamma_r\Big|_\tau = -\ln\left(\frac{\left|F_p(\omega)\right|_{\omega_r}}{\left|F_r(\omega)\right|_{\omega_r}}\right)\Big/ d\,, \qquad (9)$$

where $|F_r(\omega)|$ and $|F_p(\omega)|$ stand for the spectral amplitude at the probe frequency ω_r, corresponding to the windowed time segment τ of the signals $y_r(t)$ and $y_p(t)$. The instantaneous variations of attenuation are $\Gamma(t)$, since $\gamma_p(t)= \gamma_r(t)+ \Gamma(t)$.

Figures 2a-2c show typical recorded signals and a schematic representation of the signal processing. At overall, the signal processing consists in a sliding window that simultaneously transforms the time segment of the reference (y_r) and perturbed (y_p) signals, and computes the relative time shift (Eq. 8) and amplitude variations (Eq. 9) between them. Figures 2d-f show magnified plots of the signals. Herein, the window length was set to five cycles of the high frequency probe that corresponds to 1/69 times the resonant frequency corresponding to the first bending mode of vibration. Such a window length provides an almost constant value of acceleration (see Figure 2d). Then, time shift and amplitude variations can be precisely related to the in-plane strain which is derived from the accelerometer response (see section 2.4). Figures 2e and 2f compare a time segment of y_r and y_p, before and after an impact event. Before the impact event, the phase differences between the signals y_r and y_p are close to zero (Figure 2e), whereas they become evident after the hammer blow (Figure 2f).

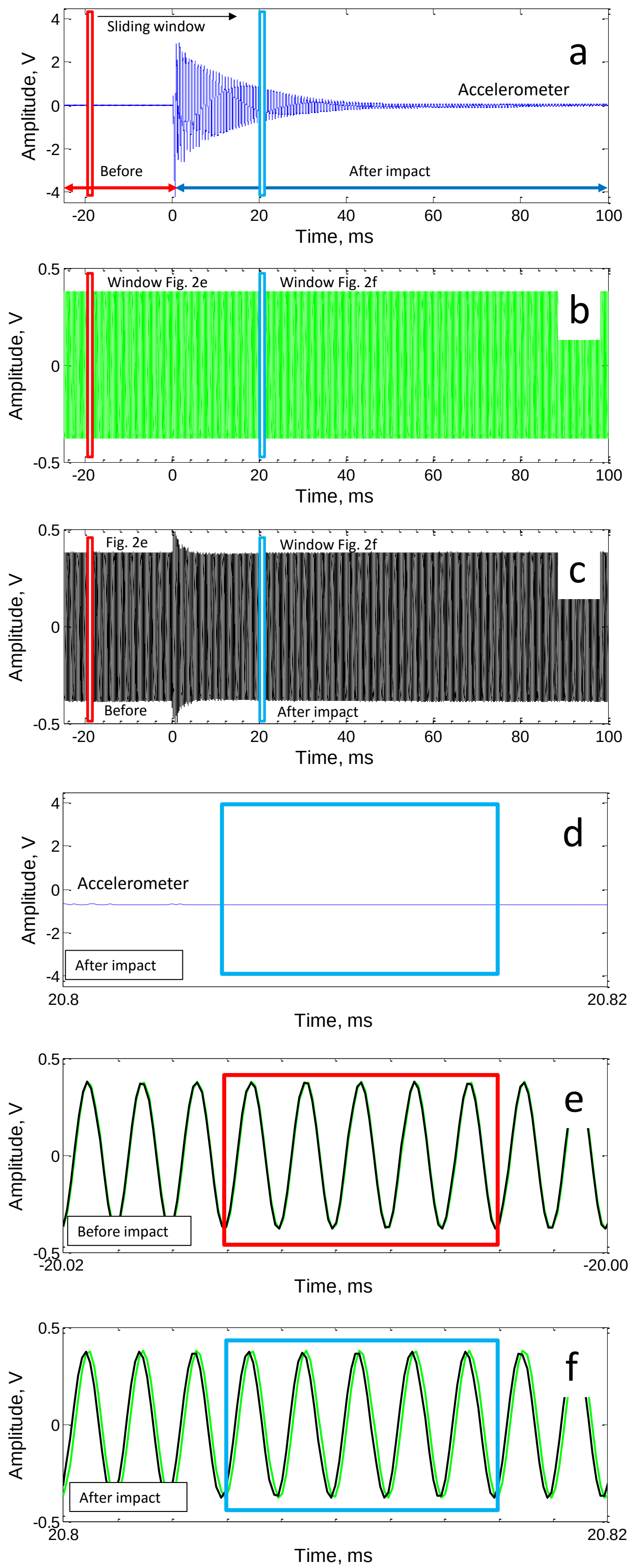

Sliding window
a
Accelerometer
Before
After impact
Amplitude, V
Time, ms
Window Fig. 2e
Window Fig. 2f
b
Fig. 2e
c
d
e
f
Before impact

1

Figure 2. (Color online) Typical time domain signals and schematic representation of the signal processing: a) signal recorded by the accelerometer, b) ultrasonic monochromatic reference signal (y_r), c) impact-modulated ultrasonic signal (y_p), d) a time segment of the acceleration signal after the hammer blow; it shows an almost constant value of acceleration (and hence strain) within the length of the window (10 μs), e) a time segment of the ultrasonic probes y_r and y_p before the hammer blow (the window is shown in red), and f) a time segment the ultrasonic probes y_r and y_p after impact (the window is shown in blue).

2.4. Measurement of strain from acceleration response

Different resonant modes are generated upon hammer blow excitation. For reference, the frequency domain spectra for the five hammer blows are represented in Figure 3a. The broadband excitation generated upon a hammer blow ranges from 0 to nearly 2 kHz. A numerical eigen-frequency analysis of linear isotropic material, and for the specific sample the geometry and material properties of the concrete sample —Mo, ν and ρ, see section 2.1— leads to the first bending mode occurring at 1449 Hz, the first torsional mode at 1981 Hz, the second bending mode at 3249 Hz, and the longitudinal mode at 3335 Hz. For the given impact point and frequency band generated, only the first bending mode (1442 Hz obtained experimentally) contributes to the strain field, and other fundamental and higher order modes will not be excited (Figures 3a and 3b).

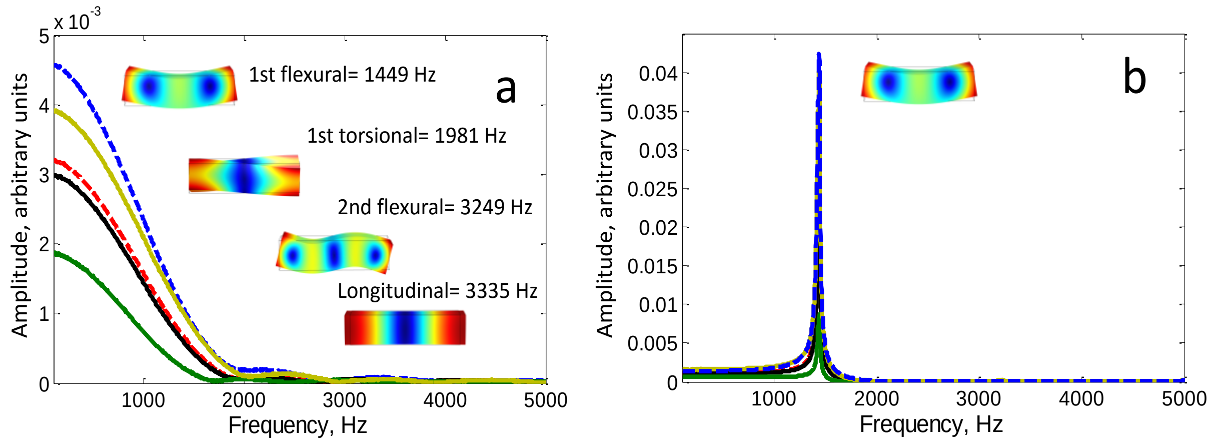

Figure 3. (Color online) a) Frequency response for the five impulse signals as acquired by the hammer load cell, and b) frequency spectra from acceleration signals. Inset figures show the mode shapes obtained by the numerical eigen-frequency analysis.

From the acceleration response, the dynamic strain on the outermost fiber of the beam owed to the first bending mode of vibration can be derived from the solution of the Euler-Bernouilli beam equation[29]. However, the assumptions of the Euler-Bernouilli beam theory do not apply in the case of short beams[30]. Alternatively, Payan and colleagues[31] proposed estimating the strain from a numerical finite element model (FEM), relating the out-of-plane acceleration (a_{zz}) to the in-plane strain (ε_{xx}); in this case that owed to the first bending mode of vibration, as

$$\varepsilon_{xx} = \frac{K \cdot \varepsilon_{num}}{K \cdot a_{zz num}} \cdot a_{zz \exp} \quad ; \tag{10}$$

where K is an amplification factor used by the FEM software to display relative values of strain and acceleration in the solution of free boundary conditions. The factor K is then divided out, ε_{num} and $a_{zz,num}$ are the in-plane strain and out-of-plane acceleration obtained in the eigen-frequency analysis; $a_{zz,exp}$ is the out-of-plane acceleration obtained experimentally. In the following, we use the convention of negative strains for compression of the material.

3. Results and discussion

Figures 4a-d show representative results of the relative variations of time shift and the variation of signal attenuation as the mechanical energy input naturally decreases. The results reveal a sudden softening of the material produced after a hammer blow, which manifests as a decrease of material modulus and an increase of attenuation (decrease of signal amplitude). The instantaneous variations of both extracted signals —derived from Eqs. 8 and 9, and shown in Figures 4a and 4c— are mainly driven by the first resonant bending mode of the sample, and harmonics at twice the fundamental resonance frequency. Simultaneously, the signals are instantaneously offset because of the non-classical contributions: the fast and slow hysteretic motions. For better understanding of the classical and non-classical contributions, the signals were decomposed, to untangle the effect of material conditioning from the relative variation of time shift and the variation of attenuation properties: C_E and C_D respectively. Such decomposition can be attained by applying a low pass filter to the resulting time shift and amplitude variation signals[13]. Herein, the cutoff frequency was set to 1/3 of the low frequency excitation. The instantaneous offsets ($C_E(t)$ and $C_D(t)$) were then subtracted from the whole time shift and amplitude variation curves. Such decomposition allows one to analyze separately the relaxation kernel (material conditioning) after a hammer blow, and the instantaneous modification of the classical material nonlinearity (β and δ) with decreasing strain amplitude ($\Delta\varepsilon$). Once the relaxation kernels (the instantaneous offsets C_E and C_D) of the signals have been untangled, the resulting mean-centered variations of the time shift signal include the low frequency excitation ($h=1$), and H harmonics (see Figure 4e). The resulting signal can be described as

$$-2\cdot\frac{\Delta t}{t_0}(t)-C_E(t)=\sum_{h=1}^{h=H}A_p e^{ih\omega_M\cdot t+\xi_h\cdot t}\,, \tag{11}$$

where A_p is the amplitude of the signal corresponding to the harmonic h; the variable ξ_h takes into account the decaying energy for every harmonic h of the relative variation of modulus (see inset plot in Figure 4e). On other hand, the strain owed to the first bending mode resonant frequency (ω_M) can be described as

$$\varepsilon_{xx}(t)=S_1\cdot e^{i\omega_M\cdot t+\xi_M\cdot t}\,, \tag{12}$$

where S_1 is the amplitude of the strain signal (see Figure 4d), and ξ_M is the modal damping ratio. For simplicity, Eqs. 11 and 12 do not consider time-dependent frequency and attenuation behavior, which are normally observed during the ring down of the signals in concrete[32,33]. After substituting Eq. 11 and Eq. 12 into Eq. 5, a relative quantification of the classical higher order terms can be obtained as $\beta'=A_1/S_1$ and $\delta'=A_2/S_1^2$. Herein, the amplitudes A_1, A_2, and S_1 were estimated using a sliding window that computes the spectral amplitude over ten cycles of their corresponding signals (Figures 4e and 4f). Therefore, these amplitudes are weighted averaged values obtained through a Fourier transform. The obtained values are β'= -300 and δ'= -7.4·10^7, within the strain amplitudes of S_1=3·10^{-6} and 1·10^{-6}. Such analysis leads to similar values of β' and δ' and C_E obtained through a second order polynomial fit of the relation between the relative time shift (as $-2\cdot\Delta t/t_o$) and strain (see polynomial fit in Figure 4b). The main drawback of the polynomial fit method[14,18-20], is the lack of fit of the second order polynomial to the observed behavior (Figure 4b), and hence, a Fourier analysis can be preferred. However, the amplitudes A_1, A_2 and S_1 obtained from the Fourier analysis of transient response signals are weighted averaged values of the actual amplitude, which can result in an underestimation of the actual amplitudes.

Normally, the relation between time shift variations and strain resembles a bow tie, and likewise for the attenuation variations, since both signals are delayed in phase with respect to the strain signal (Figures 4b and 4d). Such phase delay depends on the storage and loss modulus of the material, namely the relation between the real and imaginary parts of the frequency domain signals[34], as well as on the hysteretic contribution $U(\Delta\varepsilon, \dot{\varepsilon})$. Further, by integrating the relation between the relative variations of modulus with strain, the stress-strain relationship can be obtained as

$$\sigma(\varepsilon) = \sigma_L(\varepsilon) + \sigma_{NL}(\varepsilon) = M_o \cdot \varepsilon + M_o \int \frac{\Delta M}{M_o} \cdot d\varepsilon \,, \qquad (13)$$

where σ_L and σ_{NL} are the linear and nonlinear contributions to the stress-strain relationship. However, because of the relative characteristic of the measure of material nonlinearity conducted herein, the nonlinear stress-strain counterpart can be quantified as

$$\sigma'_{NL}(\varepsilon) = \int -2 \cdot \frac{\Delta t}{t_0} \cdot d\varepsilon \,, \qquad (14)$$

where the nonlinear stress counterpart σ_{NL} is proportional to σ'_{NL} (results shown in Figure 4g). On other hand, the energy dissipated (ΔE) during a hysteretic stress-strain cycle, because of internal friction, can be quantified as[35]

$$\frac{\Delta E}{E_o} = \frac{\oint \sigma_{NL} \cdot d\varepsilon}{M_o \varepsilon^2} \,, \qquad (15)$$

where E_o is the elastic energy stored in the specimen when the strain is a maximum. The results obtained from the analysis conducted through Eqs. 14 and 15 show how the hysteretic behavior progressively vanishes, as a measure that the strain amplitude decreases. As a result, the energy dissipated in every cycle (Figure 4h) decreases with decreasing strain amplitude.

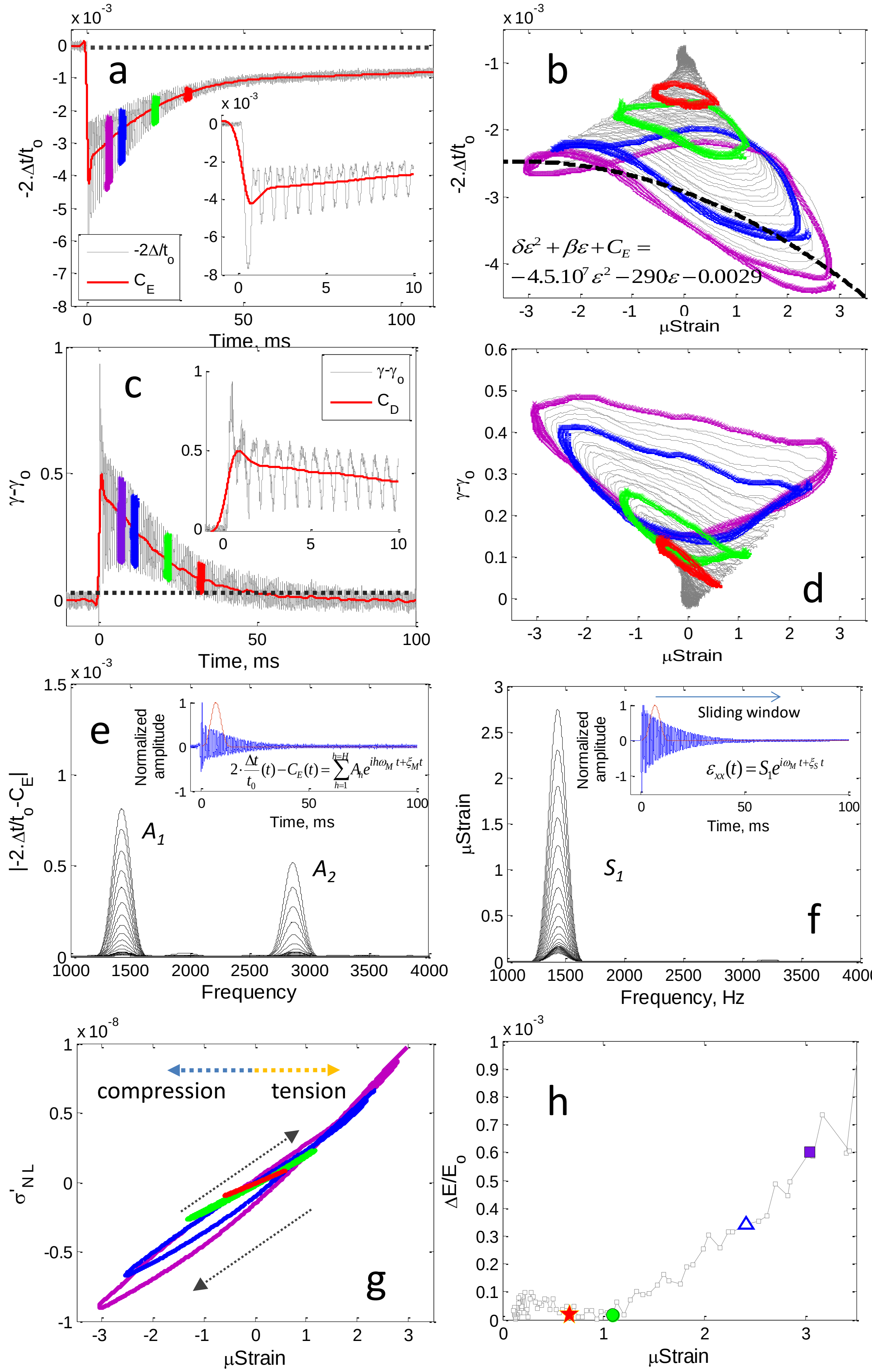
a
b
c
d
e
f
g
h
-2.Δt/t_o
C_E
Time, ms
μStrain
$\delta\varepsilon^2+\beta\varepsilon+C_E=$
$-4.5.10^7\varepsilon^2-290\varepsilon-0.0029$
γ-γ_o
C_D
|-2.Δt/t_o-C_E|
Normalized amplitude
$2\cdot\frac{\Delta t}{t_0}(t)-C_E(t)=\sum_{h=1}^{h=H}A_h e^{ih\omega_M t+\xi_M t}$
A_1
A_2
Frequency
Sliding window
$\varepsilon_{xx}(t)=S_1 e^{i\omega_M t+\xi_S t}$
S_1
Frequency, Hz
compression
tension
σ'_NL
ΔE/E_o

1

Figure 4. (Color online) Dynamic properties extracted for a single impact (force = 4.7 kN): a) relative variation of time shift as a function of time; inset plot shows the cyclic response whose frequency matches the first bending mode of vibration, b) relative variations of time shift as a function of strain; dashed line shows a second order polynomial fit as $-2\cdot\Delta t/t_o = \delta' \cdot \varepsilon^2 + \beta' \cdot \varepsilon + C_E$, c) variation of ultrasonic attenuation with time, d) variation of ultrasonic attenuation as a function of strain, e) untangled mean-centered variations of the relative variations of time shift (Eq. 11) in frequency domain, and analyzed in short windows of 10 cycles; inset plot shows the corresponding time domain signal and the sliding window, f) strain signal in frequency domain, g) relative nonlinear stress (σ'_{NL})-strain relationship derived from Eq. 14, and h) specific loss (Eq. 15) as a consequence of the hysteretic behavior. Dashed lines in a) and c) show that the recovery of the modulus takes a longer time than that found for the variation of the ultrasonic attenuation.

When the material is investigated at different impact energies, the same behavior as presented in Figure 4 is consistently reproduced (results not shown here). However, the more energy is introduced by the hammer blow, the more the material modulus and attenuation are offset. Figures 5a and 5b show the maximum offset of the relaxation kernels ($C_{E,min}$ and $C_{D,max}$, shown as square symbols), and the behavior of C_E and C_D as a function of the strain amplitude during the ring down. As regards the elastic softening of the material, it is observed that the minimum value of C_E at every impact exhibits an inverse proportionality to the attained strain amplitude as

$$\min\{C_E(\Delta\varepsilon)\} = \alpha_{CE} \cdot \Delta\varepsilon \,, \qquad (16)$$

which leads to a value of α_{CE} = -800. This approach is in fact equivalent to the nonlinear resonance spectroscopy-based techniques (Eq. 3), since the variable C_E represents the time-averaged relative variations of modulus ($\Delta M/M_o$), as shown in previous studies[18]. However, the behavior of $C_E(\Delta\varepsilon)$ and $C_D(\Delta\varepsilon)$ observed during ring down differs from the simple observation of their maximum absolute offsets (Eq. 16 and Figures 5a and 5b), most likely because of the contribution of the slow dynamic effect. Similar results were anticipated by Van Damme and Van Den Abeele[36] in the investigation of fatigue damage in carbon fiber-reinforced polymer plates. In that study, the dependence between resonant frequency and strain amplitude followed different trends when the material nonlinearity was investigated at increasing excitation amplitudes, and when it was investigated through the analysis of the ring down of the sample (see Figure 3 in Van Damme and Van Den Abeele[36]). These findings suggest that the relaxation of the elastic properties after a nonlinear dynamic excitation is the result of the coupled mechanisms of fast and slow hysteretic motions. Therefore, the instantaneous variations of the resonant frequency during the ring down of the sample are a consequence of the attained strain amplitude at every impact, as well as of the past history load[37].

Fast motion hysteresis is thought to be driven by the recovery of asperities that are eventually broken during the strain field generated on resonance of the sample[38]. Conversely, a different volume of asperities remains in metastable equilibrium once the dynamic excitation vanishes, and will return to the initial state because of thermal fluctuations[38] and other mechanisms not yet established[11] which takes place on a longer timescale (slow dynamics). Since the two mechanisms seem to coexist during a dynamic excitation[10], the elastic softening C_E can be written as the superposition of fast and slow contributions as

$$C_E = C_{E,fast} + C_{E,slow}; \tag{17}$$

and analogously for C_D. If it is assumed that the fast hysteretic motion is mainly driven by the onset of the strain amplitude signal, the relaxation kernel owed to slow hysteretic motion ($C_{E,slow}$) can be found by scaling the envelope of the strain amplitude —in the case that only one resonant mode dominates the dynamic response— and subtracting it from the total contribution as

$$C_{E,slow} = C_E - \min\{C_E\} \cdot \frac{\Delta\varepsilon(t)}{\Delta\varepsilon_{\max}}. \tag{18}$$

We can therefore assume that the fast dynamic effect ($C_{E,fast}$) is proportional to the strain amplitude —as shown in Eq. 16—while the deviation of the proportionality behavior of C_E is gathered in the variable $C_{E,slow}$. The value of α_{CE} after untangling the slow dynamic contribution for a single impact is α_{CE} = -710 (Figure 5c), and approximately the same for every different hammer blow. Interestingly, these values are close to those obtained through the quantification of α_{CE} from the minimum offset obtained for five impacts (Eq.16). Likewise for the analysis conducted on C_D (Figures 5b and 5d). Therefore, after the slow dynamics of a single impact are untangled, the estimation of the parameter α approximates to the value obtained with a nonlinear resonant spectroscopy approach, wherein the effect of the slow dynamics is minimized[10]. The contribution of the slow dynamics becomes more evident when the signals are shown as a function of time. Figures 5e and 5f show the untangled fast and slow hysteretic effects on the relaxation kernels as a function of time. The fast counterpart is the scaled envelope of the strain signal (Eq. 18), while the slow contribution directs the global behavior of the relaxation kernels, C_E and C_D, away from the scaled strain signal envelope. Remarkably, the slow dynamic contribution seems to be enhanced on C_E compared with C_D. This observation is not unique.

Similar behavior was also observed in compressional mode DAET experiments conducted on rock[17]. Although more research is needed in this respect, the fast hysteretic motion is most likely captured by the attenuation variation (C_D) which recovers completely to the initial properties, γ_o (Figure 5f), at the time that the strain signal is completely damped. This observation suggests that the underlying mechanisms of slow dynamics differ in the recovery processes of the elastic and attenuation properties.

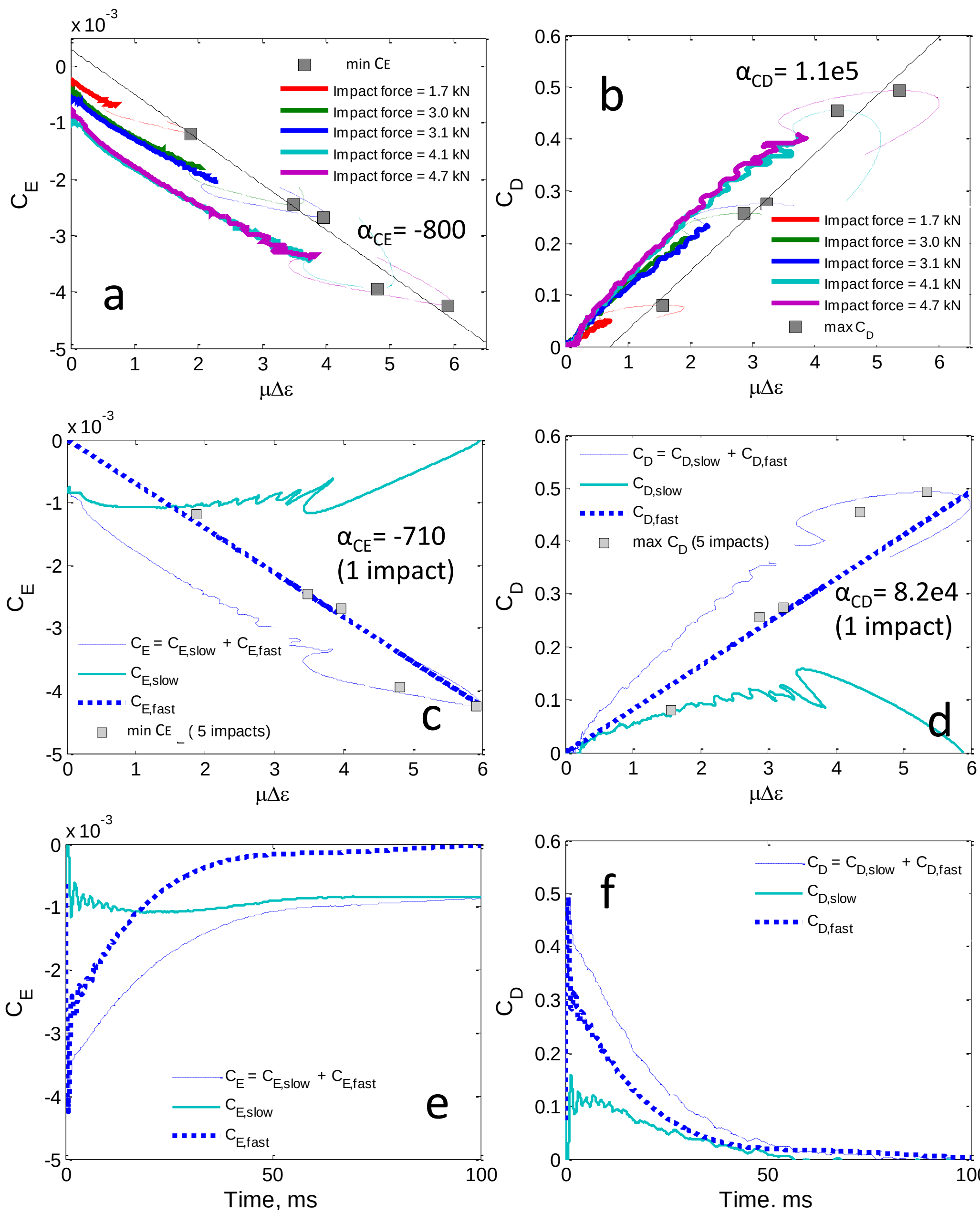

Figure 5. Relaxation kernel observed for five different impact energies, for a) the elastic properties (C_E) for five different impact energies, b) the attenuation properties (C_D). Untangled fast and slow dynamic contributions from a single impact as a function of strain amplitude, for c) C_E and d) C_D, and untangled fast and slow dynamic contributions from a single impact as a function of time, for e) C_E, and f) C_D.

Despite only one concrete sample was tested herein, the extent of material nonlinearity is reasonable for undamaged concrete when compared with previous studies[31-33]. We expect however, that the full range of nonlinear characteristics extracted herein be enhanced as a measure that cracking-like damage progresses. To this end, prospective work will focus in assessing distributed microcracking damage and surface-breaking cracks in concrete samples. On other hand, the methodology proposed in this study can be transposed to various applications which involve non-steady-state vibration, such as the analysis of earth response during ground motion, in structure health monitoring applications by using ambient noise, as well as on-site assessment of infrastructure materials, where usually only one face is available for nondestructive inspection. Some of these applications were previously devised in other studies[21,22]. However, the approach and analysis conducted here allows a more detailed description of the material nonlinearity.

4. Conclusions

This study shows the feasibility of extracting the full nonlinear behavior of materials by using a hammer blow to modulate a continuous high frequency probe. The approach was demonstrated in one undamaged concrete sample. The analysis focused on investigating the amplitude and phase changes produced in the continuous probe wave upon transient vibration. The extracted dynamic features in this study are those expected for materials that present distributed contact-like defects such as concrete or rocks: 1) the relative variations of modulus with strain resembled a bow tie, 2) the modulus decreased and progressively was recovered with the onset of the strain amplitude, and 3) the modulus was not completely recovered at the time that the strain amplitude was completely damped. Consequently, these phenomena were also reproduced on the attenuation properties. In addition, the recoveries of modulus and attenuation properties (C_E and C_D) during the ring down of the sample were analyzed. The analysis consisted in decomposing the modulus and attenuation recoveries in those contributions strictly proportional to the strain amplitude (fast dynamic effect), and those that directed away from such proportional relationship the recoveries (slow dynamic effect). After untangling the slow dynamic contribution, the hysteretic parameters (α_{CE} and α_{CD}) obtained from a single impact event were similar to those obtained from a nonlinear resonant spectroscopy based approach; that is obtaining the hysteretic parameters from multiple impact events.

Acknowledgments

The authors want to acknowledge the financial support of the Ministerio de Economia y Competitividad (MINECO), Spain and FEDER funding (Ondacem Project: BIA 2010-19933). J.N. Eiras is grateful to the Ministerio de Economía y Competitividad (MINECO), Spain, grant BES-2011-044624 and grant EEBB I-15-10178, in support of an extended visit to the Aix-Marseille Université. The French National Research Agency is also thanked for support under the EVADEOS (grant ANR-11-VILD-0002) and ENDE (grant ANR-11 RSNR 0009) programs.

References

1. Johnson PA, Jia X. Nonlinear dynamics, granular media and dynamic earthquake triggering. *Nature*. 2005;437(7060):871-874.
2. Callé S, Moreschi H, Renaud G, Defontaine M. Ultrasound propagation in trabecular bone: A numerical study of the influence of microcracks. *Ultrasonics*. 2014;54(5):1231-1236.

3. Barguet L, Pezerat C, Bentahar M, El Guerjouma R, Tournat V. Ultrasonic evaluation of the morphological characteristics of metallic powders in the context of mechanical alloying. *Ultrasonics*. 2015;60:11-18.

4. Nagy PB. Fatigue damage assesstment by nonlinear ultrasonic materials characterization. *Ultrasonics*. 1998;36:375-381.

5. Guyer RA, Johnson PA. Nonlinear Mesoscopic Elasticity: Evidence for a new class of materials. *Phys Today*. 1999;52(4):30-36.

6. Solodov IY, Krohn N, Busse G. CAN: an example of nonclassical acoustic nonlinearity in solids. *Ultrasonics*. 2002;40(1-8):621-625.

7. Kazakov V V., Sutin A, Johnson P A. Sensitive imaging of an elastic nonlinear wave-scattering source in a solid. *Appl Phys Lett*. 2002;81(4):646.

8. Van Den Abeele K, Carmeliet J, Ten Cate JA, Johnson PA. Nonlinear Elastic Wave Spectroscopy (NEWS) Techniques to Discern Material Damage, Part II: Single-Mode Nonlinear Resonance Acoustic Spectroscopy. *Res Nondestruct Eval* 2000;12:31-42.

9. Pasqualini D, Heitmann K, TenCate JA., Habib S, Higdon D, Johnson PA. Nonequilibrium and nonlinear dynamics in Berea and Fontainebleau sandstones: Low-strain regime. *J Geophys Res*. 2007;112(B1):B01204.

10. Johnson PA, Sutin A. Slow dynamics and anomalous nonlinear fast dynamics in diverse solids. *J Acoust Soc Am.* 2005;117(1):124-130.

11. Johnson PA. Nonequilibrium Nonlinear-Dynamics in Solids : State of the Art State of the Art in Nonequilibrium Dynamics. In: Delsanto PP, ed. *Universality of Nonclassical Nonlinearity*. New York: Springer; 2006:49-69.

12. Renaud G, Callé S, Remenieras J, Defontaine M. Exploration of trabecular bone nonlinear elasticity using time of flight modulation. *IEEE Trans Ultrason Ferroelectr Freq Control*. 2008;55(7):1-10.

13. Rivière J, Renaud G, Guyer RA, Johnson PA. Pump and probe waves in dynamic acousto-elasticity: Comprehensive description and comparison with nonlinear elastic theories. *J Appl Phys*. 2013;114(5):054905.

14. Renaud G, Le Bas P-Y, Johnson PA. Revealing highly complex elastic nonlinear (anelastic) behavior of Earth materials applying a new probe: Dynamic acoustoelastic testing. *J Geophys Res.* 2012;117(B06202):1-17.

15. Paultre P, Proulx J, Talbot M. Dynamic testing procedures for highway bridges using traffic loads. *J Struct Eng.* 2005;121(2):362-376.

16. Yang Y-B, Lin CW, Yau JD. Extracting bridge frequencies from the dynamic response of a passing vehicle. *J Sound Vibr* 2004;272:471-493.

17. Moradi-Marani F, Kodjo SA, Rivard P, Lamarche CP. Application of the mechanical perturbation produced by traffic as a new approach of nonlinear acoustic technique for detecting microcracks in the concrete: A laboratory simulation. *AIP Conf. Proc*. 2012; 1430:1493–1499.

18. Renaud G, Rivière J, Haupert S, Laugier P. Anisotropy of dynamic acoustoelasticity in limestone, influence of conditioning, and comparison with nonlinear resonance spectroscopy. *J Acoust Soc Am*. 2013;133(6):3706-3718.

19. Renaud G, Rivière J, Le Bas P-Y, Johnson PA. Hysteretic nonlinear elasticity of Berea sandstone at low-vibrational strain revealed by dynamic acousto-elastic testing. *J Acoust Soc Am.* 2013;40(4):715:719.

20. Rivière J, Shokouhi P, Guyer RA, Johnson PA. A set of measures for the systematic classification of the nonlinear elastic behavior of disparate rocks. *J Geophys Res Solid Earth*. 2015;120:1-18.

21. Bui D, Kodjo SA, Rivard P, Fournier B. Evaluation of Concrete Distributed Cracks by Ultrasonic Travel Time Shift Under an External Mechanical Perturbation: Study of Indirect and Semi-direct Transmission Configurations. *J Nondestruct Eval*. 2013;32(1):25-36.

22. Moradi-Marani F, Kodjo SA, Rivard P, Lamarge C-P. Nonlinear Acoustic Technique of Time Shift for Evaluation of Alkali-Silica Reaction Damage in Concrete Structures. *ACI Materials Journal*. 2014;111:1-12.

23. Fröjd P, Ulriksen P. Amplitude and phase measurements of continuous diffuse fields for structural health monitoring of concrete structures. *NDT&E Int.* 2016;77:35-41.

24. Payan C, Garnier V, Moysan J, Johnson PA. Determination of third order elastic constants in a complex solid applying coda wave interferometry. *Appl Phys Lett*. 2009;94(1):011904.

25. Quiviger A, Payan C, Chaix J-F, Garnier V, Salin J. Effect of the presence and size of a real macro-crack on diffuse ultrasound in concrete. *NDT&E Int.* 2012;45:128-132.

26. Naik TR, Malhorta VM, Popovics JS. The Ultrasonic Pulse Velocity Method. In: Malhorta VM and Carino NJ, ed. *Handbook on Nondestructive Testing of Concrete*. 2nd Edition, Boca Raton: CRC Press; 2004:181-199.

27. Turgut P, Kucuk OF. Comparative Relationships of Direct, Indirect, and Semi-Direct Ultrasonic Pulse Velocity Measurements in Concrete. *Russian J Nondestruct Eval*. 2006;42(11):745-751.

28. Donskoy D, Sutin A, Ekimov A. Nonlinear acoustic interaction on contact interfaces and its use for nondestructive testing. *NDT&E Int.* 2001;34(4):231:238.

29. Hunt FV. Stress and strain limits on the attainable velocity in mechanical vibration. *J Acoust Soc Am.* 1960;32(7):1123-1128.

30. Gérandin M, Ryxen D. *Mechanical Vibrations: Theory and Application to Structural Dynamics*. New York: John Wiley & Sons, 1997.

31. Payan C, Ulrich T J, Le Bas P Y, Saleh TA, Guimaraes M. Quantitative linear and nonlinear resonance inspection techniques and analysis for material characterization: Application to concrete thermal damage. *J Acoust Soc Am.* 2014;136(2):537-546.

32. Eiras JN, Monzó J, Payá J, Kundu T, Popovics JS. Non-classical nonlinear feature extraction form standard resonance vibration data for damage detection. *J Acoust Soc Am.* 2014;135(2):EL82-EL87.

33. Dahlén U, Ryden N, Jakobsson A. Damage identification in concrete using impact non-linear reverberation spectroscopy. *NDT&E Int.* 2015;75:15-25.

34. Trarieux C, Callé S, Moreschi H, Renaud G, Defontaine M. Modeling nonlinear viscoelasticity in dynamic acoustoelasticity. *Appl Phys Lett*. 2014;105(26):264103.

35. Kolsky H. *Stress Waves in Solids*. New York: Dover, 1963.

36. Van Damme B, Van Den Abeele K. The application of nonlinear reverberation spectroscopy for the detection of localized fatigue damage. *J Nondestruct Eval*. 2014;33:263-268.

37. Scalerandi M, Gliozzi AS, Bruno CLE, Antonaci P. Nonequilibrium and hysteresis in solids: Disentangling conditioning from nonlinear elasticity. *Phys Rev B - Condens Matter Mater Phys*. 2010;81:1-7.

38. Lebedev A V., Ostrovsky LA. A unified model of hysteresis and long-time relaxation in heterogeneous materials. *Acoust Phys*. 2014;60(5):555-561.